EXPERIMENTAL SPATIO-TEMPORAL STRUCTURE OF VORTICAL AND STRAINING REGIONS NEAR THE WALL OF OPEN-CHANNEL FLOW.

J. C. Wells[1] & Y. Yamamoto[2]

[1]Member, JSCE, Ph.D., Faculty of Science and Engineering, Ritsumeikan University
(Noji Higashi 1-1-1, Kusatsu, Shiga 525-8577 Japan)
[2] Ph.D., Research Fellow, Faculty of Science and Engineering, Ritsumeikan University,
currently Research Assistant, Faculty of Engineering, Kansai University
(Yamate-cho 3-3-35, Suita, Osaka 564-8680 Japan)

High-resolution videographic P.I.V. is applied to measure cross-stream velocity components at 15 Hz and 1 Hz in the lower half of a smooth-bed open channel flow at $Re_* = u_* d / \nu = 300$ (where d is the flow depth of 10.0 cm). We emphasize analysis of the quantity $Q_x=(\omega_x^2 - S_x^2)/2$ (ω_x : streamwise vorticity, S_x : rate of strain in the cross-stream plane) which expresses the relative strength of rotational and straining motion in the illuminated plane. Instantaneous flow fields, confirmed by two-point correlations, show that regions of negative Q_x lie above, below, or beside regions of strongly positive Q_x. Isosurfaces of a suitably conditioned spatio-temporal correlation of Q_x reveals a tilt and inclination of streamwise vortices ("SV") which agrees substantially with previous results from DNS [*e.g.* Stretch (1990), Jeong *at al.*(1997)], and suggest a consistent lattice-type spatial relationship with neighboring SV.

Key Words : *turbulent flow, open channel, streamwise vortex, particle image velocimetry*

1. INTRODUCTION

Based on a data base from DNS of closed channel flow, Stretch[1)] proposed a staggered typical arrangement of Streamwise Vortices ("SV") in turbulent channel flow, as shown in Fig. 1. (*cf.* Jeong *et al.* [2)]). Since DNS of open-channel flow[3)] suggests that turbulence structure near the wall does not depend on the presence of a free surface, one infers that similar structures should be important in open-channel flow. Experimentally, Particle Image Velocimetry ("PIV") measurements in near-wall horizontal planes of an open-channel flow of water have revealed the presence of staggered arrangements of wall-*normal* vorticity[4)]. In the present work, high-resolution videographic P.I.V., with illumination in the *cross-stream* plane, is applied to measure cross-stream velocity components at 15 Hz and 1 Hz in the lower half of a smooth-bed open channel flow at $Re_* = u_* d/\nu = 300$ (d: flow depth = 10.0 cm; width 50 cm; 5.5 m from channel entrance). Based on such measurements, and on dye visualizations, we claimed in reference (5) to provide the first direct evidence for Stretch's staggered arrangement of SV. This communication presents spatio-temporal correlations associated with SV structure, and considers the relationship between vortex cores and their associated straining regions.

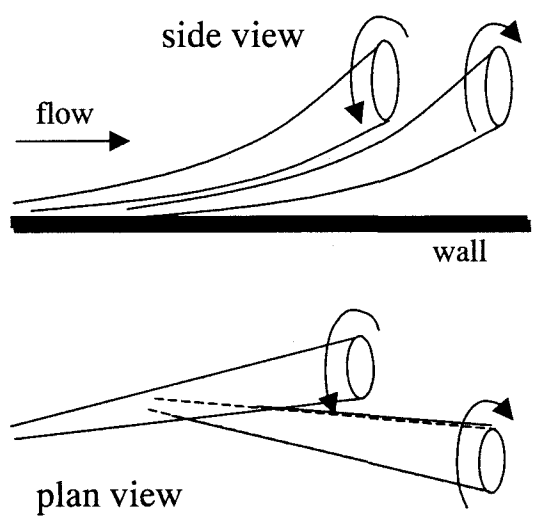

Fig. 1. Sketch of dominant near-wall vortex structure, following Stretch[1)]

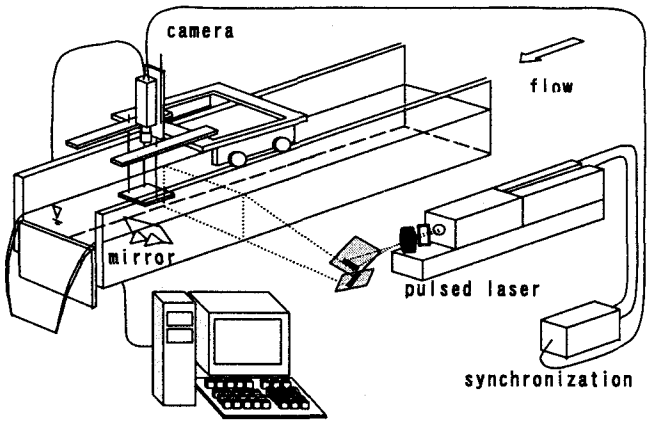

Fig. 2. Sketch of flow channel and flow visualization apparatus.

2. METHOD

We have performed particle image velocimetry ("PIV") in smooth-bed open channel flow at $Re_* = u_* d / \nu = 300$, equivalent to a bulk flow Reynolds number of $U d / \nu = 5250$. The apparatus is shown in Fig. 2. Flow depth d was 10.0 cm; the channel width and length are respectively 50 *cm* and 8 *m*. A 5 *mm* thick double-pulsed laser sheet was produced by a double Nd-YAG laser (Quantel S.A., France) run at 15 *Hz*, illuminating a cross-stream plane 5.5 *m* from the channel entrance. 1K*1K video images were recorded by a Kodak ES1.0 progressive-scan camera (Nikkor 105 *mm* microlens) looking upstream through a mirror bottom-mounted at 50 *cm* downstream of the light sheet, and through a glass window over the mirror at the water surface. Light pulses from one laser were synchronised with a 250 *ms* exposure of the camera; pulses from the second laser were triggered 5 *ms* later, in the next camera exposure; velocity fields were thus obtained at 15 *Hz*. The delay of 5 *ms* was sufficiently short that no streamwise shift of the light sheet was required between the two pulses. Near-neutrally buoyant 10 μm diameter hollow glass spheres (Sphericel powder, Potters Industries, USA) served as flow tracers. The field of view was 4.96 *cm* wide * 4.69 *cm* high, so that only the lower half of the channel was observed. Cross-stream velocity components were calculated by maximising the cross-correlation of 49*49 pixel templates between image pairs. Tests with a rotating clear plastic plate simulating the particle-laden fluid showed that streamwise vorticity could be estimated with acceptable accuracy by first smoothing velocity vectors with the 9 surrounding values.

The bottom-mounted mirror was 10cm * 10 cm, and blocked nearly the entire flow depth over a width of 10 cm. Thus it is possible that some deceleration of the flow was occurring in the measurement section, which could be expected to lead to increased turbulence intensity. However profiles of r.m.s. wall-normal velocity taken by the above technique, and by auxiliary runs with the light sheet in the streamwise vertical (x-y)plane and the mirror removed, showed profiles that were indistinguishable to within the uncertainty, approximately $\pm 3\%$.

3. CORRELATIONS

Coordinate System. Herein we denote the downstream direction by x, the wall-normal direction by y, and the span direction by z (right-hand rule).

The following analysis concentrates on the quantity Q_x , defined by

$$Q_x = (\omega_x^2 - S_x^2)/2 \quad ,$$

where ω_x is streamwise vorticity and S_x is the rate of strain in the cross-stream plane:

$$\omega_x = \frac{\partial v}{\partial z} - \frac{\partial w}{\partial y} \qquad S_x = \frac{\partial v}{\partial z} + \frac{\partial w}{\partial y}$$

Q_x reflects the relative importance of rotational motion and straining motion; where Q_x is strongly positive, we think of the motion in the cross-stream plane as being "vortical"., while negative values indicate a region where strain dominates vorticity. Q_x can be interpreted as a component of the second invariant of the deformation rate tensor $Q = \frac{\partial u_j}{\partial x_i}\frac{\partial u_i}{\partial x_j}$, which is half the source term in the Poisson equation for pressure obtained by taking the divergence of the N-S equations in incompressible flow.

(1) Spatial correlations

Figure 3 shows two-point correlations C_f for spatial separations in the illuminated plane, defined for $f = \omega_x$, Q_x by:

$$C_f(y,\Delta z,\Delta y) = \frac{\int\int f(z,y,t) f(z+\Delta z, y+\Delta y, t)\,dz\,dt}{(f-\bar{f})_{rms}(y)(f-\bar{f})_{rms}(y+\Delta y)} \qquad (1)$$

in which $\int dt$ denotes averaging over 350 velocity fields recorded at 1 *Hz* so as to provide nearly independent samples. The correlations C_ω (graphs a,b,c) have an elliptical form in the near field. The

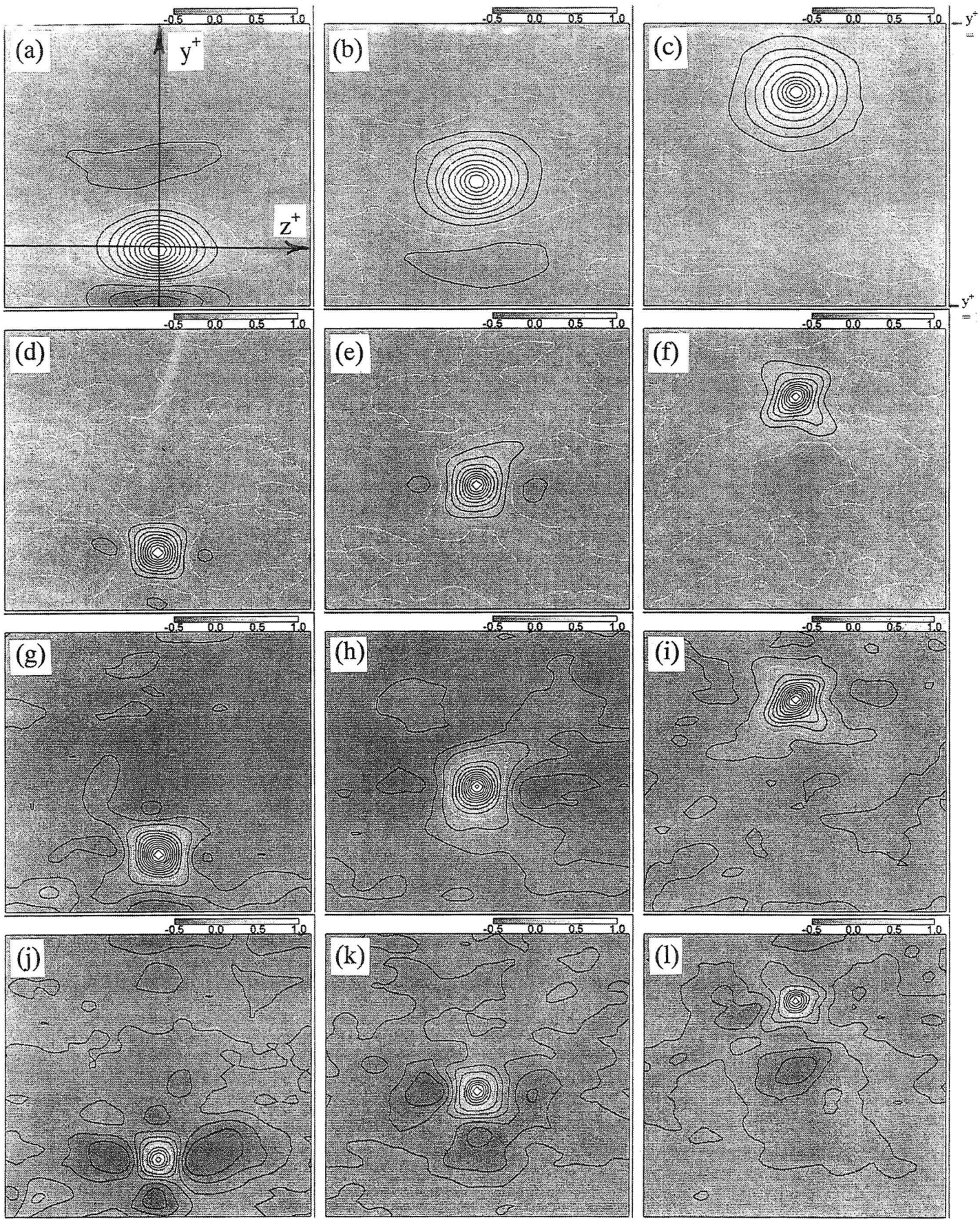

Fig. 3 Two-point correlations C_f for spatial separations in the illuminated plane (equ. 1), with height of base points indicated at top of figure, and axes as shown in (a); (a-c) $f = \omega_x$;(d-l) $f = Q_x$, (d-f) unconditional, (g-i) conditional on Q_x ,>0 at base point, (j-l) conditional on $Q_x < 0$ at base point. White curves indicate zero correlation.

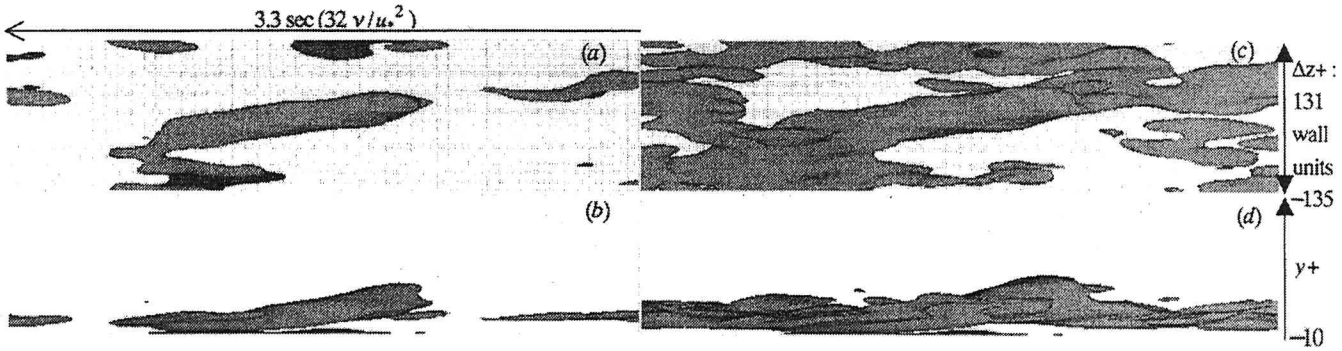

Fig. 4. Spatiotemporal correlation coefficient of Q_x'conditional on Q_x >0 at base point, with samples reflected about base point in span direction when ω_x <0, top (a,c) and side(b,d) view. Threshold for dark grey is 0, light grey: (a,b) .15, (c,d) 0.11.

far field shows some evidence of a diamond pattern[5], but this pattern is rather weak, and has not been found to be very consistent from one experiment to another. On the other hand, the correlations C_Q (graphs d,e,f) clearly show preferred directions at roughly $\pm 45^O$ to the vertical which are consistently apparent over the range of fixed points y^+ between 30 and 100 . The structure of the correlation changes significantly when contributions to the integral (equation 1) are conditioned on $Q_x >$ 0 at the base point *(y,z)* of the correlation (graphs g,h,i) or on $Q_x < 0$ (graphs j,k,l). Most strikingly, correlations conditioned on $Q_x < 0$ at the base point (*i.e.* strain rate dominating rotation) show a very strong tendency for a region of positive Q_x , *i.e.* a vortical region, to lie either to the side or underneath the base point. We will return to this aspect when examining a particular instance of the flow in section 4.

(2) Spatio-temporal correlations

Figure 4 shows isosurfaces of the spatiotemporal correlation of Q_x, admitting only samples with positive values of Q_x at the base point *(y,z)*, and with individual flow realizations reflected in the spanwise direction for $\omega_x < 0$ at the base point; these surfaces should reveal the statistically dominant structure near a streamwise vortex (of positive vorticity; assuming symmetry the structure near an SV of negative sign will be the reflection of that in the figure). Correlations were calculated from 3 runs at 15 *Hz*, each of 350 velocity fields. The higher threshold for C_Q in (a) and (b) reveals a tilt and inclination of the vortex core which agrees substantially with previous results from DNS[1),2)]. A lower threshold (c,d) reveals a tendency for a lattice-type spatial relationship with neighboring SV when viewed from above (c). However, there is no indication of a vortex above the base point, and no inclination of *neighboring* vortical structures in the *x-y* plane is suggested by the isosurface at this threshold. These observations thus contrast with the typical structure proposed by Stretch[1)].

4.ANALYSIS OF TYPICAL FLOW FIELDS

To help interpret the differences between the spatial correlations of ω_x and Q_x (Fig. 3), Figure 5 shows two instantaneous cross-stream velocity fields, separated by 1.2 *s* (= 12 ν / u_*^2) that exemplify two common patterns of vorticity. The first snapshot (a) is characterized by narrow "jets" rising at about 45 degrees from horizontal, switching from oblique left to oblique right, and snaking between vorticity concentrations of opposite sign. The vorticity field at this instant (c) has a structure of orthogonal ribs, joined together at T-junctions, that is reflected in the oblique rectangular aspect of the instantaneous two-point vorticity correlation C_ω' whose origin is scanned over the entire instantaneous field;

$$C'_\omega(\Delta x,\Delta y,y,t) = \frac{\int \omega(x,y,t)\omega(x+\Delta x,y+\Delta y,t)dy\,dz}{\omega^2_{rms}(y,z)} \qquad (2)$$

(In fact, such oblique vorticity correlation is more commonly observed to show banding in a single direction instead of two near-orthogonal directions.) Similar remarks apply to the field of Q_x, shown in graph (g), and corresponding correlation C_Q' (graph h) at this instant. Observations of instantaneous vorticity fields frequently reveal such an oblique pattern. Our impression is that such patterns occur as arrangements of somewhat weak vorticity patches. When stronger structures appear, their orientations and relative positioning seem to be much more varied.

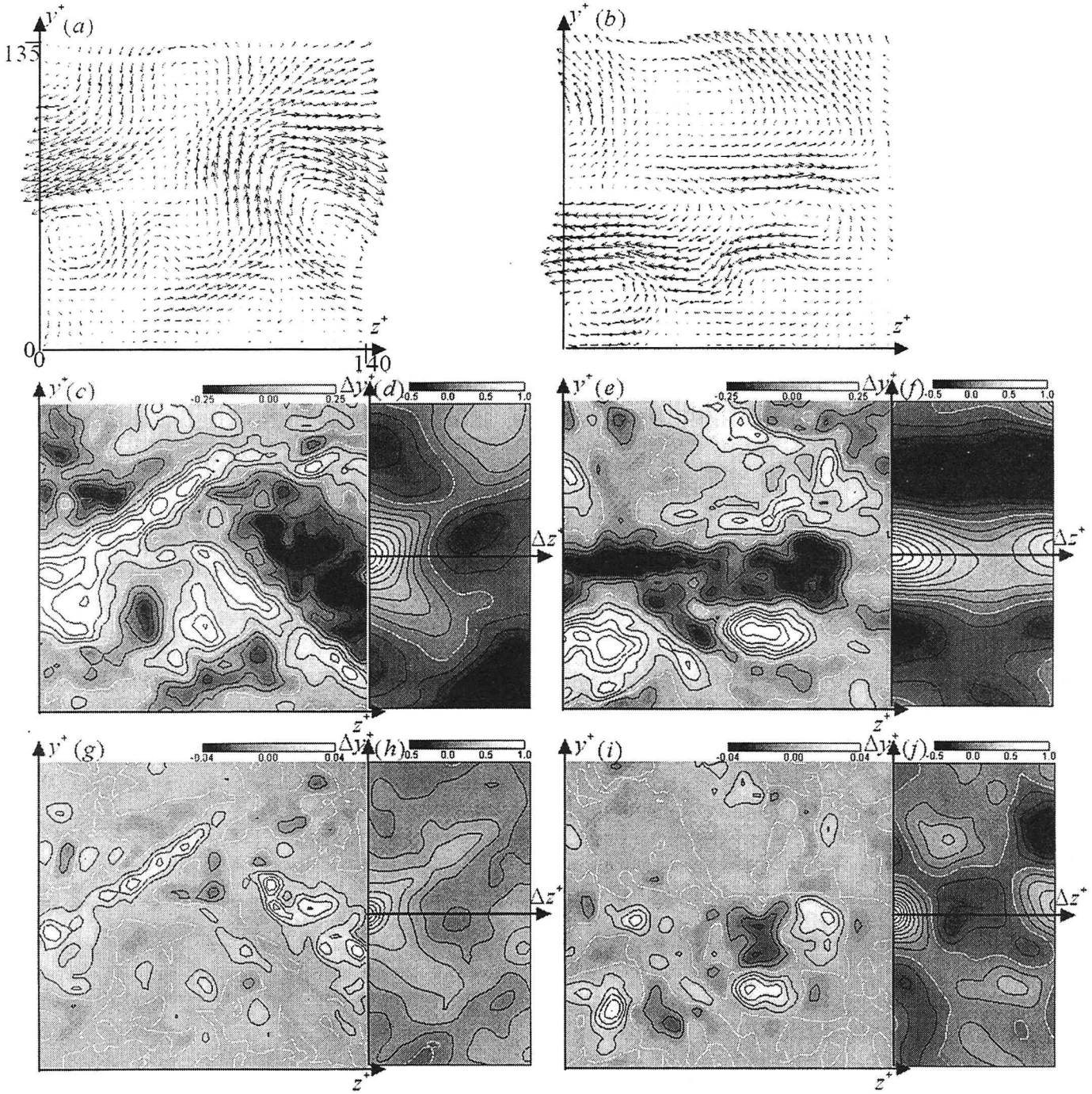

Fig. 5. Instantaneous velocity maps (a,b), and associated quantities at two instants (indicated by dashed lines in fig. 6) separated by $\Delta t = 1.2$ s ($\Delta t^+ = 12$). (c,e):instantaneous maps of ω_x^+ (contour interval of 0.05 wall units, zero contour in white); (g,i): instantaneous maps of Q_x^+ (contour interval of 0.008 wall units, zero contour in white); (d,f): instantaneous two-point correlations C_ω' of ω_x over each sample (*cf.* equation (2) (contour interval 0.1, zero contour in white); (h,j): corresponding instantaneous correlations of Q_x (contour interval 0.1, zero contour in white) }

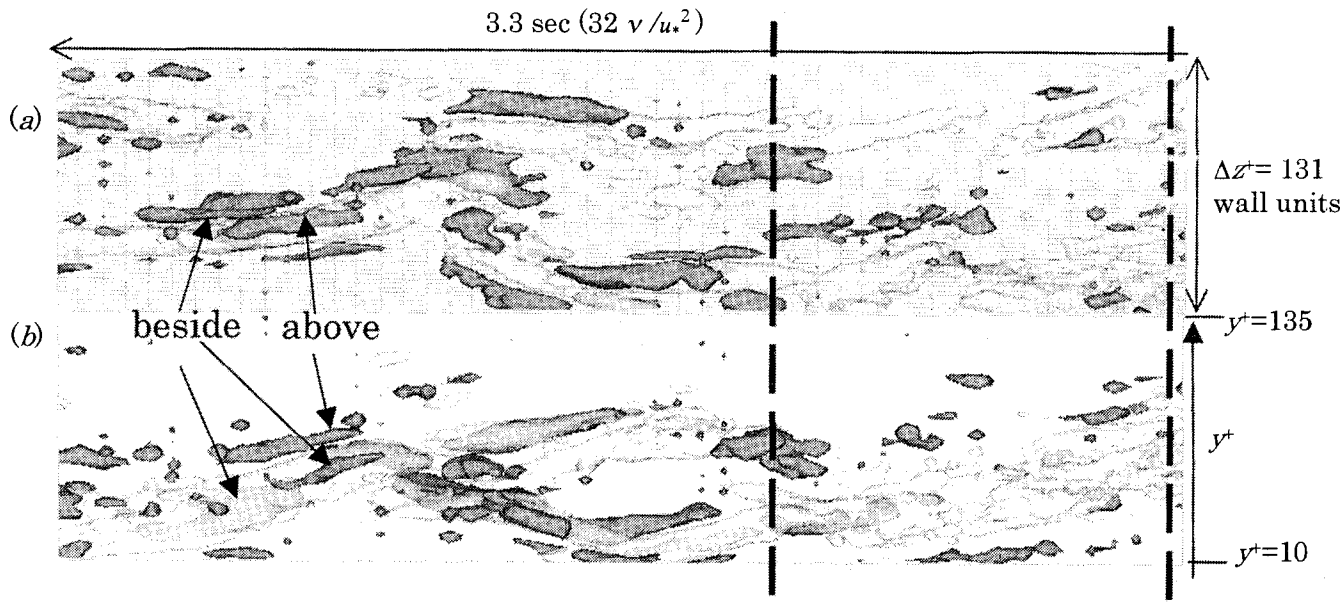

Fig. 6. Spatiotemporal structure of Q_x from continuous recording at 15 velocity samples/sec, isosurfaces Q_x^+= 0.25 (semitransparent) and Q_x^+= -0.20 (grey) seen in top view (above) and side view (below). Flow from left to right (time increases from right to left). Dashed line on right corresponds to the flow field on the left of Fig. 5; the dashed line towards the center corresponds to the right of Fig. 5.

Another common pattern of instantaneous vorticity correlation C_ω', that of horizontal banding, is seen in Fig. 5(f). The correlation of Q_x at this instant, shown in (j), retains the oblique checkerboard character observed in (h). This contrast in the behavior of C_Q' and C_ω' reflects the very different forms of the two-point correlations C_ω and C_Q seen in Fig. 3.

In Figure 6,the spatio-temporal structure of Q_x during a 3.3 *s* segment of a run at 15 Hz is displayed *via* isosurfaces in a three-dimensional plot. Nearly all regions of negative Q_x lie above, below, or beside regions of strongly positive Q_x, in agreement with the statistical tendency shown in Fig. 3(i,j,k).

7. CONCLUSION

Concentrating on analysis of the quantity Q_x, in particular two-point correlations in the cross-stream plane, we have provided additional evidence that there is an oblique aspect of turbulent boundary layer structure when viewed in the cross-stream plane, as hypothesized in our earlier work[5].

Based on dye-vizualization[5] and on time-resolved measurements of vorticity *etc.* in the cross-stream plane (*cf.* Fig. 4), we feel that there should be a certain quasi-periodic aspect to the inclined structures contributing to these correlations. In future work, we would now like to find a quantitative tool that will reveal such temporal aspects of boundary-layer structure.

On the matter of instrumentation, we are now performing stereo experiments with two CCD cameras, so as to measure all three components of velocity in the light sheet.

ACKNOWLEDGEMENTS: This research has been supported in part by grants from the Monbusho Gakujutsu Frontier program, and Monbusho Grants-in-aid for Scientific Research C (lead researcher; J. Wells). We thank Messrs. Takashima and Ukai for assistance with PIV experiments.

REFERENCES

1) Stretch, D. Automated Pattern Eduction from Turbulent Flow Diagnostics, Center for Turbulence Research Annual Research Briefs, 1990
2) Jeong, J., Hussain, F. Schoppa, W. and Kim, J. Coherent Structures near the wall in a Turbulent Channel Flow *J. Fluid Mech.*. Vol. 332, pp. 185-214, 1997
3) Nagaosa, R. Direct numerical simulation of vortex structures and turbulent scalar transfer across a free surface in a fully developed turbulence. *Physics Fluids,* Vol. 11(6), pp. 1581-1595, 1999
4) Ueno, T. and Utami, T.: Three-dimensional flow visualization of coherent structures of turbulence in an open-channel flow. *Proceedings, Ninth Symposium on Turbulent Shear Flows.* Kyoto, Japan, 1993
5) Wells, J.C., Yamane, Y., Yamamoto, Y., Egashira, S. and Nakagawa, H. Dye visualization and P.I.V. analysis of streamwise vorticity structure in a smooth-bed open-channel flow. *Annual J. Hydr. Eng., JSCE* Vol. 44, pp. 491-496, 2000

(Received October 2, 2000)